# Thermal properties and degradation kinetics of epoxy-$\gamma$-alumina and epoxy-zinc oxide lightweight composites

N. Camacho[a,*], J.F. May-Crespo[b], J.B. Rojas-Trigos[c], K. Martínez[c], E. Marín[c] and G.C. Mondragón-Rodríguez[d]
[a]*CONACYT-CIDESI-CENTA, National Center of Aeronautical Technologies,*
*Carretera Estatal 200 Querétaro-Tequisquiapan Km. 23, No. 2254, Localidad Galeras, 76270,*
*Parque Aeroespacial Querétaro. Colón, Querétaro, México.*
*[*]e-mail: nayeli.camacho@cidesi.edu.mx*
[b]*CONACYT -El Colegio de Michoacán,*
*Cerro de Nahuatzen 85, Fracc. Jardines del Cerro Grande, La Piedad, Michoacán, 59370, México.*
[c]*Instituto Politécnico Nacional, CICATA-Legaria,*
*Calzada Legaria No. 694 Col. Irrigación, Miguel Hidalgo, 11500, Ciudad de México, México.*
[d]*CONACyT, Center of Engineering and Industrial Development, CIDESI, Surface Engineering Department,*
*Querétaro, Av. Pie de la Cuesta 702, 76125 Santiago de Querétaro, México.*

Lightweight composite materials are the gold standard in aeronautical and aerospace applications due to their strength and low mass. To transport higher payloads and reduce launching costs, nanosatellites, an excellent option for space exploration due to their lightweight structures, are migrating to composite materials. Nanosatellites, also known as CubeSats, must resist high thermal radiation loads while working in orbit. Polymer-based composite materials maintain low mass and the incorporation of reinforcing ceramic fillers contributes to increasing radiation and heat resistance, meeting both requirements. In this work, the effects of $\gamma$-alumina ($Al_2O_3$) and zinc oxide (ZnO) micro- and nanoparticles on the thermal properties and degradation kinetics of epoxy-based composites were investigated. The effective thermal conductivity improved up to 17.8 % for epoxy/$\gamma$-$Al_2O_3$ and 27.4% for epoxy/ZnO. The effective thermal diffusivity values show a monotonic decreasing behavior as a function of the particle concentration for the epoxy/$\gamma$-$Al_2O_3$ composites while for the epoxy/ZnO composites, no correlation on the effective thermal diffusivity values with the ZnO-content was observed. Both oxide-based ceramic fillers increase the thermal stability of epoxy up to 250°C; however, $\gamma$-$Al_2O_3$ decreased the maxima decomposition temperature of the epoxy matrix by 6°C. Zinc oxide did not affect the maxima decomposition temperature but decreased the activation energy of epoxy by 45%. These results provide a feasible manufacturing method for epoxy-based composite materials (*i.e.*, nanosatellites) where efficient heat transfer, heat resistance, and low mass are required.

*Keywords:* Epoxy-based composites; oxide ceramic fillers; thermal stability; thermal conductivity.

## 1. Introduction

In the last decades, nanosatellites, also called CubeSats, have transformed the landscape of space missions, especially for Earth orbit exploration. Nanosatellites have also been widely used as technology demonstrators, scientific tools, and for educational purposes [1,2,3]. The design of the nanosatellite structures considers minimizing the weight without sacrificing performance because it is technically convenient to accommodate higher payloads and to maintain or even reduce the cost of the launch. The recommended structural materials for the development of CubeSats - [3,4] - include Al-7075-T73 and Al-6061-T6 alloys, due to their strength, weight, and coefficient of thermal expansion [5]. Alternatively, a few scientific groups have started to explore the use of composite materials for the fabrication of the panels constituting nanosatellites [2,6], an example being the Swiss-Cube, launched in 2009 [7], that included carbon fiber-epoxy composite panels in its structural subsystem. Composite materials have a lower density than aluminum alloys and represent a viable candidate to replace aluminum in some of the

structural subsystems of the nanosatellites if thermal property requirements are met [8,9]. According to Corpino *et al.* [4], one of the most critical issues for nanosatellite missions is the effect of the thermal environment on the nanosatellite material. Heat transfer phenomena (direct solar radiation, albedo, earth infrared radiation (IR), and internal heat generation due to on-board electronics) in space are mainly regulated by thermal conduction and radiation [4]. Therefore, one of the most challenging issues is for the material to manage temperature variations ranging from 100°C to - 130°C corresponding to exposure to direct sunlight and eclipse phases in extremely short periods [1]. The current thermal properties of polymeric matrices used in the manufacturing of composite materials need to be improved to comply with the required standard for the construction of CubeSats.

Polymer-based composite materials reinforced with ceramic filler powders offer a diversity of possible multifunctional applications [10,11]. Several functional properties such as electrical conductivity, piezoelectricity, thermal conductivity, and thermal stability can be improved, with the addition of reinforcing particles [12]. Epoxy resins, used as the

matrix of carbon fiber composites for aerospace, aeronautical, and automotive applications [13], have been combined with a variety of fillers at high and relatively low particle loadings such as graphene (1, 3, and 5 wt. %) [14], graphene oxide at 0.5 wt. % [15], carbon nanotubes at 1 and 6.1 wt. % [16,17], barium titanate at 6 wt. % [18], alumina from 1 to 70 wt. % [19-22] or combinations of these nanoparticles [17,23] to improve fracture toughness, electrical properties, flame retardancy, UV-shielding [24], and wear resistance [20]. Few studies have focused on the study of thermal properties. Y. Feng *et al*. [25] proved that the incorporation of $Al_2O_3$ particles induces an enhancement of the thermal conductivity of epoxy with increments of 145, 200, and 317 % at 50, 60, and 70 wt. % filler loading, respectively. M. Wasim Akhtar et al. also reported an increase in the thermal conductivity of epoxy with increasing filler loading up to 50 wt. % [26]. Both studies concluded that high particle loading (up to 70 wt. %) must be employed to obtain an apparent functional property improvement, which in turn, increases the weight of the material, decreases the specific mechanical properties, and turns the polymer fragile [22].

To design ceramic reinforced composite materials for nanosatellite structures, it is essential to improve the thermal properties (*i.e.*, the thermal diffusivity and conductivity) of the epoxy resins without considerably increasing the weight of composite materials. The present investigation reports the effect of micro- and nanoparticle low concentrations < 1 wt. % of $\gamma$-alumina ($Al_2O_3$) and zinc oxide (ZnO) on the thermal conductivity, stability, and kinetics degradation of an aeronautical grade biphasic epoxy resin system (Epolam 2500). The active thermography technique was employed to determine the thermal diffusivity at room temperature while the thermal conductivity of each composite was determined from the analysis of the transient thermal response. For each particle filler, the effect of the oxide nanoparticles on the thermal stability of the composite was assessed through degradation kinetics by thermogravimetric analysis.

## 2. Materials and methods

### 2.1. Particle preparation

The ZnO particles were prepared following the aqueous sol-gel synthesis method. Briefly, zinc acetate and oxalic acid were mixed at a molar concentration ratio of 0.1 /0.1 (M). The oxalic acid solution was added dropwise to the zinc acid solution, which was kept under constant agitation for 90 min (formation of the gel). The gel obtained was dried for 12 h at 60°C and then subjected to a thermal treatment at 600°C for 3 h.

The alumina particles were prepared by the citrate route. A polymeric citrate precursor derived from a citric acid aluminum nitrate solution at a molar concentration ratio of 0.5/0.1 (M) was used. The precursor thermal decomposition at 60°C formed a precipitate that was dried at 200°C for 2 h, followed by thermal treatment at 900°C for 2 h. The

synthesized ZnO and $Al_2O_3$ particles were characterized in a SmartLab XRD diffractometer from Rigaku in PB/PSA mode Parallel Beam/Parallel Slit Analyzer with a grazing incidence angle ($\omega = 0.5°$) $2\theta$ geometry and Cu K$\alpha$ radiation(40 kV, 44 Amp) at a step size of 0.04°. The diffraction patterns were indexed using the Integrated X-ray powder diffraction Software PDXL from Rigaku. The surface morphology of the synthesized powders was determined through a field emission scanning electron microscope (FE-SEM) Jeol JMS-7200F, using an accelerating voltage of 1.5 kV and different amplification factors.

### 2.2. Composite preparation

The resin compound Epolam 2500, a biphasic epoxy resin composed of primer and hardener was purchased from Sika Advanced Resins®. The primer and hardener were mixed at a 100:22 weight ratio. Zinc oxide or $\gamma$-$Al_2O_3$ particles were incorporated by solution blending in the epoxy resin at concentrations of 0.1, 0.25, and 0.5 wt. %. In a first step, ZnO particles were suspended in ethanol and sonicated for about 5 min to break the agglomerates as much as possible and until a homogeneous dispersion was achieved. Then, the epoxy resin was added to the solution that was kept under constant stirring at 50°C until ethanol was completely evaporated, and apparent uniform distribution of the ZnO in the resin was attained. The same mixing strategy was followed for the $\gamma$-$Al_2O_3$-epoxy composite. All samples were cured at room temperature for 24 h followed by a dwelling time of 2 h at 100°C.

### 2.3. Thermal characterization

#### 2.3.1. Modulated thermal response

Thermal images were acquired through an active infrared thermography setup, consisting of a TTL controllable laser (120 mW LASER LDCU5, at 658 nm); a function generator, for the generation of the TTL control signal; a closed sample chamber; and an IR camera (FLIR, SC5000), suitable to operate in the 2.5 - 5.1 $\mu$m wavelength range. Between the IR camera and the sample chamber, a germanium window was placed to avoid undesirable contributions to the thermal images. The spherical lens is used to ensure a highly focused beam impinging on the frontal sample surface. Figure 1 displays a schematic of the active thermography system.

The capabilities of the IR camera electronics, along with its software, allow the phase-sensitive images processing and synchronization to the reference signal (from the function generator); so, there is no need for an external lock-in amplifier module. The sample chamber was kept at high vacuum ($1 \times 10^{-6}$ Torr) during the measurement using a rotatory vacuum pump (Varian Vacuum Technologies, DS 102) coupled with a turbo-molecular vacuum pump (Varian Vacuum Technologies, Turbo-V 81-AG) to avoid heat losses due to
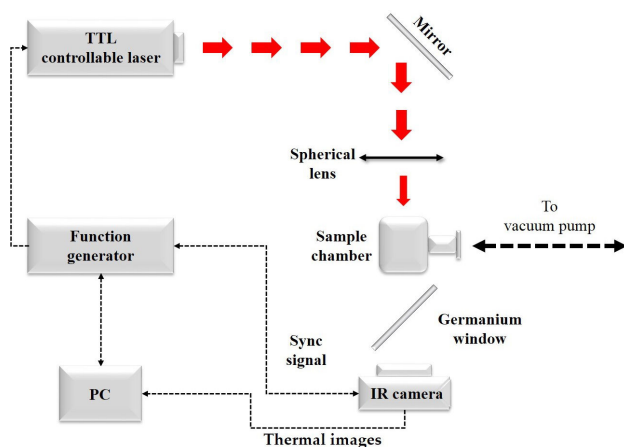
FIGURE 1. Schematic representation of the active thermography system.

conductive and convective heat transfer to the surroundings. The modulation frequency of the excitation beam was fixed to 10 mHz.

### 2.3.2. Transient thermal response

The transient thermal response of each sample was sensed using a thermal analyzer (Hot-Disk), which employs a very thin nickel wire (shaped like a double spiral, encapsulated on a 25 $\mu$m-thick Kapton cover) as the transient plane source or TPS. The TPS functions as a heating source as well as a temperature sensor through its electrical resistance time-variations. These occur when a controlled electrical power, $P_{out}$, is sustained during the time measurement, $t_{meas}$, when the TPS is in thermal contact with the studied sample. This particular technique has some resemblance to the well-known Hot-wire and Hot-strip techniques, and their mathematical foundations can be found elsewhere [27,28,29]. To avoid heat losses through the boundaries of the sample as much as possible, a $P_{out} = 25$ mW and a $t_{meas} = 10$ s were considered.

### 2.3.3. Thermogravimetric analysis

The degradation kinetics of the composites were evaluated by thermogravimetric analysis (TGA), performed in a PerkinElmer® thermogravimetric analyzer (TGA 4000) in the temperature range from 50 to 900°C, in a nitrogen flow at 20 ml·min$^{-1}$, at heating rates of 5, 10, 20 and 50°C·min$^{-1}$. Pure epoxy samples and ZnO- and $\gamma$-Al$_2$O$_3$-epoxy composites were analyzed. Samples of $18.000 \pm 0.005$ mg were placed inside the alumina sample-holder and then heated at a given heating ramp. The TGA analyses of the composites were performed under non-isothermal conditions; then, the activation energy of each composite was calculated with the Multilinear Regression Method (MLR) from the TGA data.
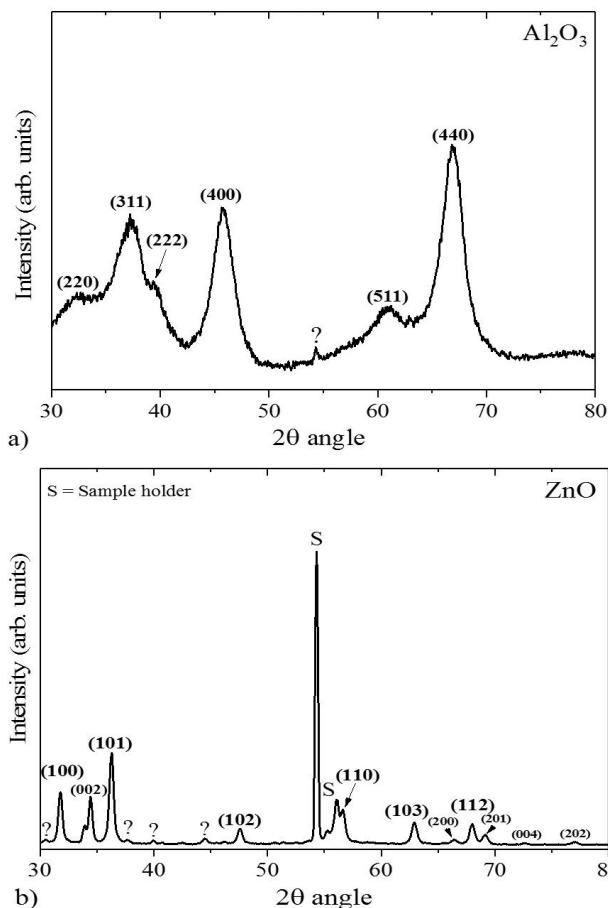


FIGURE 2. X-ray diffraction pattern recorded for the (a) $\gamma$-Al$_2$O$_3$ and (b) ZnO synthesized particles.

## 3. Results and discussion

### 3.1. Ceramic-particles characterization

The acquired X-ray diffraction patterns of the $\gamma$-Al$_2$O$_3$ and ZnO synthesized particles are presented in Figs. 2a and 2b, respectively, identifying the characteristic XRD peaks with the Miller indices of their corresponding diffraction planes. While the ZnO particles exhibit sharp (Lorentz-type) peaks (Fig. 2b) corresponding mainly to the wurtzite hexagonal phase of ZnO; the XRD obtained for the $\gamma$-Al$_2$O$_3$ particles presents broader peaks (Fig. 2a), and their positions correspond predominantly to cubic $\gamma$-Al$_2$O$_3$ [30]. The observed peaks broadening is, presumably, due to the overlapping of Lorentz-type peaks. An estimate of the crystallite size was calculated using the Rietveld method. The crystallite size of $\gamma$-Al$_2$O$_3$ particles is about 3.32 nm, while the crystallite size for ZnO particles is 22.5 nm. The apparent morphology of the obtained particles was analyzed by FE-SEM micrographs (Fig. 3). The SEM micrographs show that the ZnO powders are a combination of rod-like structures with an average thickness of 63 nm and small cubic and irregular chunks, which seem to cohere in micrometric aggregates with a max-
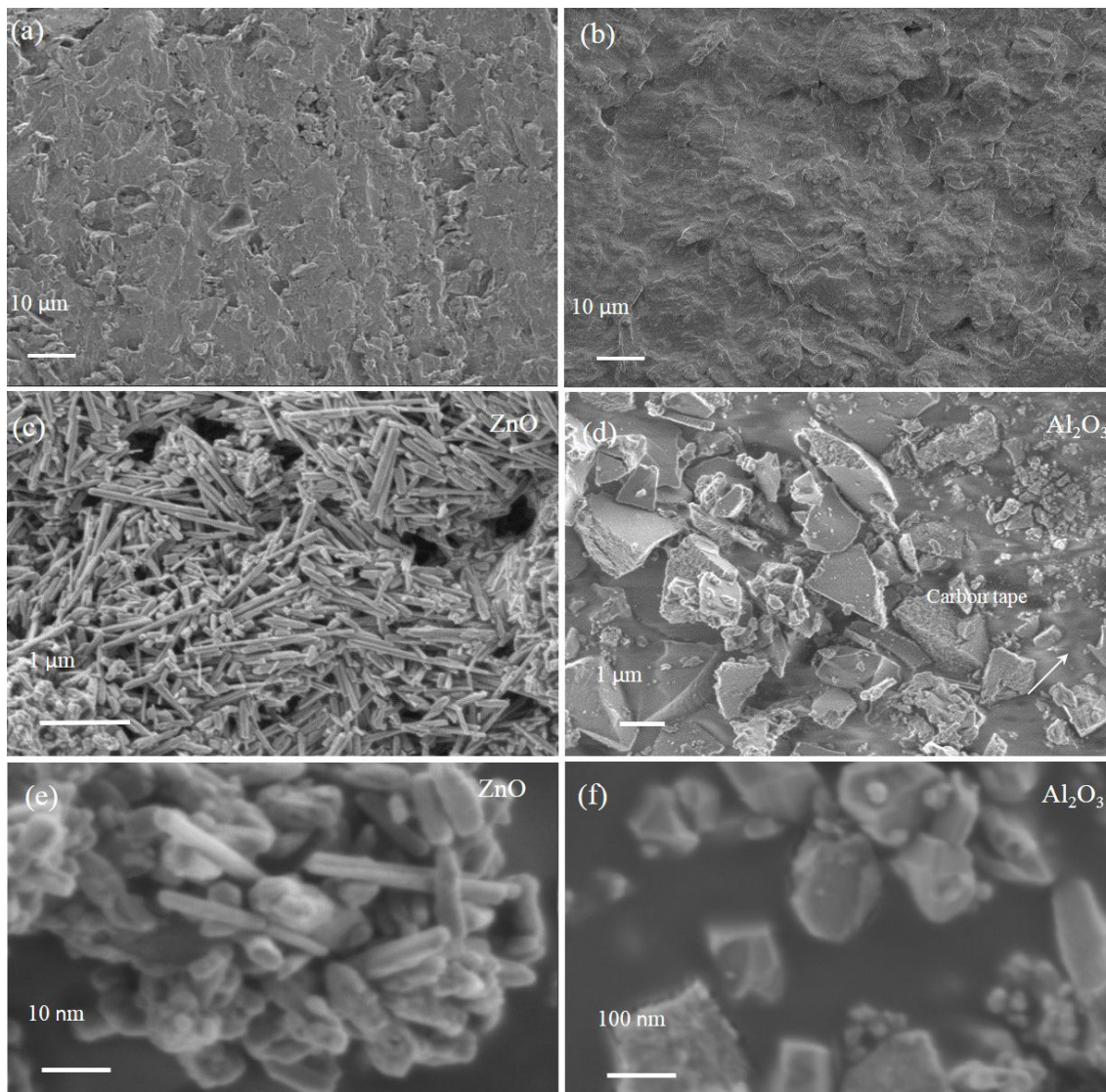
FIGURE 3. a) SEM micrographs of Epolam + 0.5 wt. % ZnO, b) Epolam + 0.5 wt. % $\gamma$-Al$_2$O$_3$, c) ZnO particles at $20kx$, d) $\gamma$-Al$_2$O$_3$ particles at $10kx$, e) ZnO particles at $80kx$, and f) $\gamma$-Al$_2$O$_3$ particles at $80kx$.

imal averaged size of 20 $\mu$m in the powder form (Figs. 3c and 3e). On the other hand, the micrographs of the $\gamma$-Al$_2$O$_3$ particles show small irregular particles, as small as 50 nm and as large as 0.22 $\mu$m, which also present a tendency to form large aggregates in the powder form (Fig. 3d and 3f). Micrographs of the composites at a concentration of 0.5 wt. %, epolam/ZnO, and epolam/$\gamma$-Al$_2$O$_3$, are presented in Fig. 3a and 3b, respectively. As it can be observed on the micrographs, the particles are not visible on the surface of the composites, and the apparent surface roughness of the epolam /$\gamma$-Al$_2$O$_3$ is higher than that of the epolam/ZnO at this particle concentration.

### 3.2. Thermophysical Properties

The slope method for thermal diffusivity measurements shows that for a homogenous thermally thin, sample the following relationship exists:

$$m_{\Delta\psi} \cdot m_{\mathrm{Ln}[\sqrt{r} \cdot \Delta T^{ac}]} = -\frac{\omega}{2\alpha_{eff}}, \qquad (1)$$

where $\Delta\psi$ is the photothermal phase shift; $\Delta T^{ac}$ is the (modulated) temperature amplitude; $r$ is the radial coordinate; and $m_{\Delta\psi}$ and $m_{\mathrm{Ln}[\sqrt{r} \cdot \Delta T^{ac}]}$ are the slopes of the linear regions in the $\Delta\psi$ versus $r$ and $\mathrm{Ln}[\sqrt{r} \cdot \Delta T^{ac}]$ versus $r$ curves, respectively [31,32,33,34,35]. From Eq. (1) the thermal diffusivity, $\alpha_{eff}$, can be obtained if the modulation frequency, $\omega$ is known. Figure 4 presents the $\Delta\psi$ vs. $r$ and $\mathrm{Ln}[r \cdot \Delta T^{ac}]$ vs. $r$ plots for the epoxy matrix. The convective-radiative heat losses at low frequencies are responsible for deviations from linearity [36].

Following the same data processing, the thermal diffusivity of the different epoxy/$\gamma$-Al$_2$O$_3$ and epoxy/ZnO composites was calculated; Figure 5 shows the results obtained. In any case, the error bars associated with the effective thermal
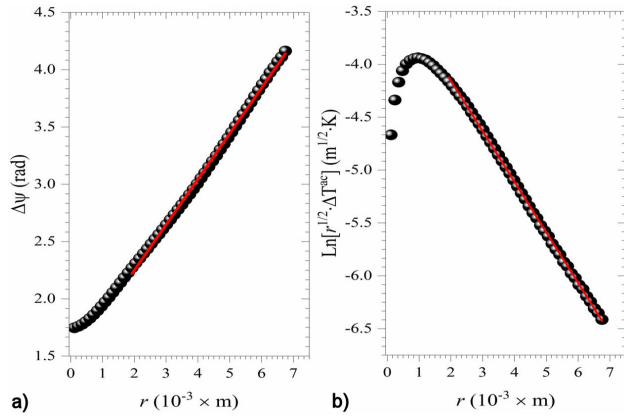
FIGURE 4. a) $\Delta\psi$ vs. $r$, and b) $Ln[\sqrt{r} \cdot \Delta T^{ac}]$ vs. $r$ plots, for the epoxy sample. The solid red line shows the best least-squares linear fit.



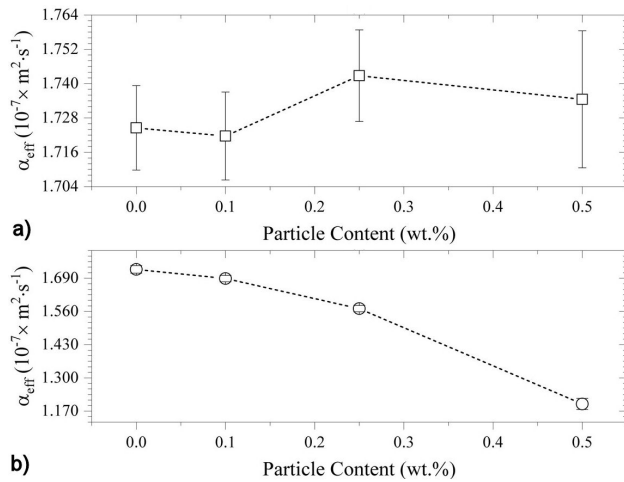FIGURE 5. Obtained values for the effective thermal diffusivity, as a function of the particle content, for (a) Epoxy/Al$_2$O$_3$, and (b) Epoxy/ZnO composites.

diffusivity are one hundred times smaller than the $\alpha_{eff}$ values ($\sim 10^{-9}$ m$^2\cdot$s$^{-1}$) for the epoxy/Al$_2$O$_3$ composites. However, for the epoxy/ZnO composites, the variations of $\alpha_{\text{eff}}$ as a function of the ZnO content are of the same order of magnitude of the corresponding error bars; therefore, the addition of ZnO has no real impact on the effective thermal diffusivity of such composite samples. On the other hand, the epoxy/$\gamma$-Al$_2$O$_3$ composites exhibit a non-linear monotonic decreasing behavior in $\alpha_{\text{eff}}$, with the $\gamma$-Al$_2$O$_3$ content. Figure 6 presents the transient thermal response of the samples under the experimental conditions described in 2.3.2 for different $\gamma$-Al$_2$O$_3$ and ZnO contents.

The effective thermal conductivity, $k_{eff}$, of the composite samples was determined from the $\Delta T$ vs. $t$ curves by linear fitting procedures according to the model reported by [29]. The obtained values for the neat epoxy matrix, epoxy/$\gamma$-Al$_2$O$_3$, and epoxy/ZnO composites agree well to similar epoxy-based composites reported elsewhere [32,33,26,37]. Figure 7 summarizes these results, indicating that the epoxy/$\gamma$-Al$_2$O$_3$ composites exhibit an increasing

monotonic behavior for $k_{eff}$ as a function of the $\gamma$-Al$_2$O$_3$ content, deviating from linearity at the origin. This supports that the oxide particle loading is well-dispersed within the matrix since dispersion has proven to be one of the most important factors to improve the thermal conductivity [26]. The improvement in thermal conductivity is recorded up to 17.8 % by introducing just 0.5 wt. % of $\gamma$-Al$_2$O$_3$. Furthermore, the improvement in thermal conductivity at such low oxide particle loading is similar to the improvement obtained by [26,47] filler loading up to 10 wt. % was added.

A quite different thermal behavior occurs for the epoxy/ZnO composites, were a non-monotonic dependency of $k_{\text{eff}}$ on the ZnO content is evident. Moreover, the sample with 0.25 wt. % content of ZnO shows an important decrease in the $k_{\text{eff}}$ value compared to the samples with 0.1 and 0.5 wt. % content of ZnO, but still higher than the $k_{\text{eff}}$ value corresponding to the neat epoxy sample. Lower conductivity at this concentration could be due to agglomerate formation at this concentration.

Considering that $k_{\text{eff}}$, $\alpha_{\text{eff}}$ are not independent thermophysical parameters, but related through the (effective) vo-
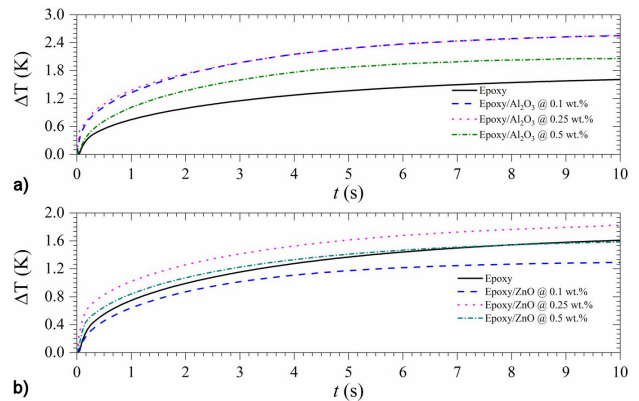


FIGURE 6. Thermal response (in amplitude) of a) Epoxy/Al$_2$O$_3$, and b) Epoxy/ZnO composites, recorded employing the Hot-Disk measurement system.
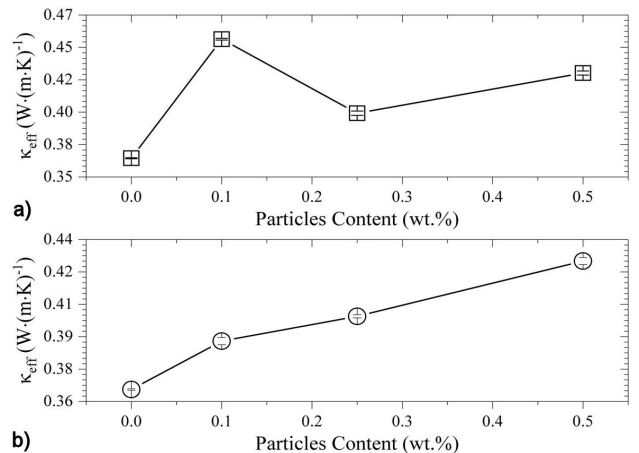


FIGURE 7. Effective thermal conductivity values of (a) Epoxy/Al$_2$O$_3$, and (b) Epoxy/ZnO composites, obtained from Hot-Disk measurement data.
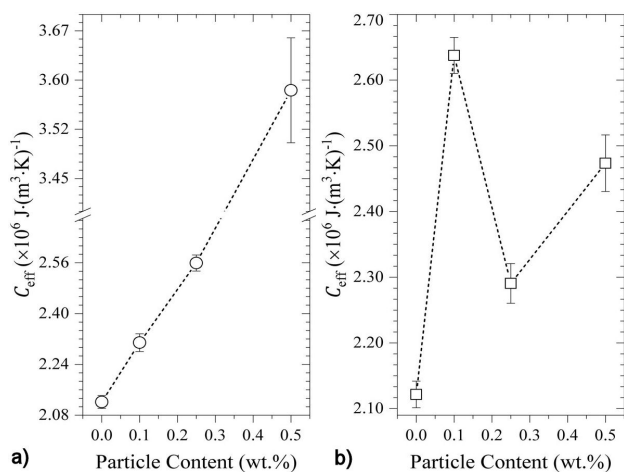
FIGURE 8.   Calculated $C_{\text{eff}}$ values of a) Epoxy/Al$_2$O$_3$, and b) Epoxy/ZnO composites, as a function of the particle content.

lume-specific heat capacity (also known as heat capacity per unit volume), $C_{\text{eff}} = k_{\text{eff}} \cdot \alpha_{\text{eff}}^{-1}$. Figure 8 displays the calculated values of $C_{\text{eff}}$ from this relation for all composite samples.

Again, the epoxy/$\gamma$-Al$_2$O$_3$ samples showed an increasing non-linear monotonic behavior in the $C_{\text{eff}}$ values as a function of the $\gamma$-Al$_2$O$_3$ content. On the other hand, the epoxy/ZnO samples show that, for a 0.25 wt. % content of ZnO, $C_{\text{eff}}$ has a local minimum mostly due to the effective thermal conductivity, since the effective thermal diffusivity values are practically the same for all the epoxy/ZnO samples here studied. Assuming that the synthesized $\gamma$-Al$_2$O$_3$ and ZnO particles are homogeneously distributed into the bulk of the sample, the effective volume-specific heat capacity could be estimated by Eq. (2) as follows:

$$C_{\text{bulk}} = \frac{\rho_{rel} \cdot w_{(d)} \cdot C_{(d)} + (1 - w_{(d)}) \cdot C_{(m)}}{1 - (1 - \rho_{\text{rel}}) \cdot w_{(p)}}. \quad (2)$$

In Eq. (2), C(m), C(d) are the volume-specific heat capacity of the continuous (neat epoxy matrix) and discrete phases ($\gamma$-Al$_2$O$_3$ and ZnO particles) of the composite, respectively; $w_{(d)}$ is the content fraction of the discrete phase, given by the wt. % particle content of the composite; and $\rho_{\text{rel}} = \rho_{(m)} \cdot \rho_{(d)}^{-1}$ is the ratio of the mass densities. However, Eq. (2) has a decreasing behavior-owing to the thermophysical properties difference between the discrete and continuous composite phases-, contrary to the experimental observation for all composites. The observed demeanor of the thermophysical properties, $\alpha_{\text{eff}}$, $k_{\text{eff}}$, and $C_{\text{eff}}$- together with the theoretical estimation $C_{\text{bulk}}$-, suggest that the ballistic heat transfer mechanism competes with the diffusive heat transfer mechanism in response to the possible formation of axial thermal paths inside the composites, being the one exception, the epoxy/ZnO composite with 0.25 wt. %. For such a particular sample, it is plausible that the concentration of ZnO particles induces the agglomeration of the particles in disjoint volume elements, diminishing the formation of thermal paths and, therefore, a greater contribution of the diffusive heat transfer mechanism

is observed. However, these hypotheses must be corroborated by quantification of the spatial distribution of the dispersed particles.

### 3.3.    Thermal stability and degradation kinetics

The thermal stability of the epoxy/$\gamma$-Al$_2$O$_3$ and epoxy/ZnO was studied by TGA at a heating rate of 10°C/min under a nitrogen atmosphere. Figure 9 displays the thermograms and their derivative (DTG) obtained for epoxy/$\gamma$-Al$_2$O$_3$ and epoxy/ZnO, respectively. As a reference, neat epoxy without ceramic particle incorporation was also analyzed. From TGA curves (Figs. 9a and 9c) of the neat epoxy, it is possible to observe that the main thermal transition occurs from 250 to 500°C with a weight loss of about to 70 %, attributed to the degradation of the epoxy network [15]. A stable zone from 500 to 700°C follows this thermal transition, and a final weight loss of about 10 % occurs from 700 to 900°C.

The total mass loss for all samples was ranged from 79.8 to 76.9 %. The derivative of the thermogravimetric curves helps to determine the temperature at which the maximum rate of thermal decomposition is reached (see Fig. 9). DTG curves displayed in Figs. 9b and 9d show a three-stage degradation for the neat epoxy in a nitrogen atmosphere, which is affected by the increasing content of each oxide. The first degradation stage of the epoxy starts at 314°C and is associated with uncured epoxy resin and loss of volatiles. The second stage of degradation onset was detected between 318 and 330°C with a maxima temperature decomposition at about 340°C; this points out to the decomposition of aromatic functional groups. The last stage observed between 480 and 550°C corresponds to the breaking of the main chains of the epoxy resin. These polymer degradation stages match with data reported in the literature [15,38,39].

The DTG curves for all composites showed that the addition of ceramic particles inhibited the first stage of the thermal degradation of epoxy, contributing to the dissipation of its volatile fraction. These findings have not been reported in other studies. The results demonstrate that for temperatures under 250°C, the addition of either ZnO or $\gamma$-Al$_2$O$_3$ with concentrations < 1 wt. % increase the thermal stability of the epoxy matrix; this is in agreement with the analysis of volatile organic compounds in polymers reported elsewhere [40]. Similar thermal transitions were observed for the second and third stages of thermal decomposition for the neat epoxy, epoxy/$\gamma$-Al$_2$O$_3$, and epoxy/ZnO, as the transitions appear at similar temperatures ranges (318–330 and 480–550°C, respectively). However, for epoxy/$\gamma$-Al$_2$O$_3$ at a concentration of 0.1 wt. %, it was noted that the third transition shifts towards lower temperatures with an onset at about 455°C.

The incorporation of $\gamma$-Al$_2$O$_3$ decreases slightly the temperature at which the maximum rate of thermal decomposition occurs from 340 to 334°C, suggesting the detriment of the thermal stability of the matrix caused by the oxide. It is believed that $\gamma$-Al$_2$O$_3$, at low concentrations, acts as a  cata-
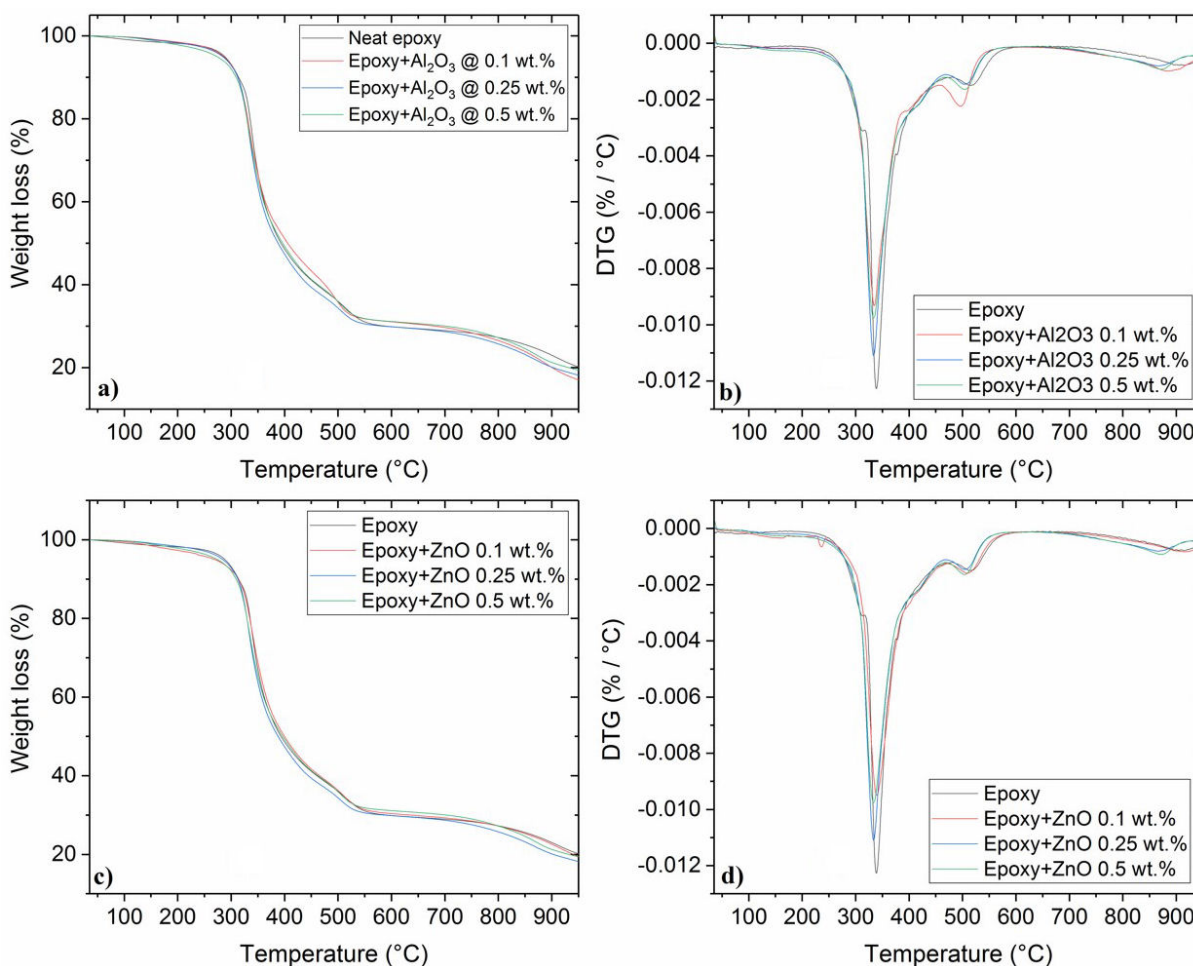
FIGURE 9. TGA thermograms for ceramic/epoxy and neat epoxy. The respective DTG thermograms for each concentration is displayed on the top right corner of the image. (a) Epoxy/Al$_2$O$_3$ and (b) Epoxy/ZnO.

lyst at high temperatures, accelerating the breaking of the polymeric chains of epoxy resin and decreasing the decomposition temperature. In the case of ZnO incorporation, the DGT curves for all concentrations showed similar thermal behavior to neat epoxy, indicating the apparent conservation of the thermal stability of the matrix.

Thermal stability factors such as initial decomposition temperature (the temperature of 5 wt. % loss, $T_{d5}$) and char

TABLE I. Thermal stability of epoxy/Al$_2$O$_3$ and epoxy/ZnO composites obtained from TGA thermograms.

| Filler | Filler content | $T_{d5}$ | Char at 900°C |
|---|---|---|---|
| | (wt. %) | (°C) | (%) |
| None | 0 | 288 | 23.08 |
| | 0.1 | 288 | 20.20 |
| γ-Al$_2$O$_3$ | 0.25 | 288 | 20.20 |
| | 0.5 | 273 | 21.34 |
| | 0.1 | 269 | 22.80 |
| ZnO | 0.25 | 269 | 22.80 |
| | 0.5 | 269 | 22.80 |

at 900°C were determined for each composite. Table I lists the thermal stability factors for both composites at different filler content. The $T_{d5}$ for epoxy/γ-Al$_2$O$_3$ at 0.1 and 0.25 wt. % was similar to that of neat epoxy. However, as the γ-Al$_2$O$_3$ content increased to 0.5 wt. %, the $T_{d5}$ decreased by 15°C. For the epoxy/ZnO, the Td5 decreased by 19°C compared to neat epoxy, regardless of the particle content. The char at 900°C decreased for both composites compared to neat epoxy. Regardless of the ZnO particle content, the char at 900°C remains constant at 22.8 wt. % while a lower concentration of γ-Al$_2$O$_3$ displays the lowest char at 900°C, 20.20 wt. %.

The thermal properties in this study are compared for epoxy resin-based composites produced by the above-mentioned process for particle loadings < 1 wt. %. The comparability of the results obtained with other studies is restricted due to differences in the epoxy resin system used; for instance, Jiang *et al.* [21] studied the behavior of epoxy (DGEBA) with contents of nano alumina (α-Al$_2$O$_3$) from 1 to 4 wt. %; the results show the $T_{d5}$ value of the composites similar to that of the neat epoxy resins (362.1°C) with char contents increasing gradually with increasing concentrations
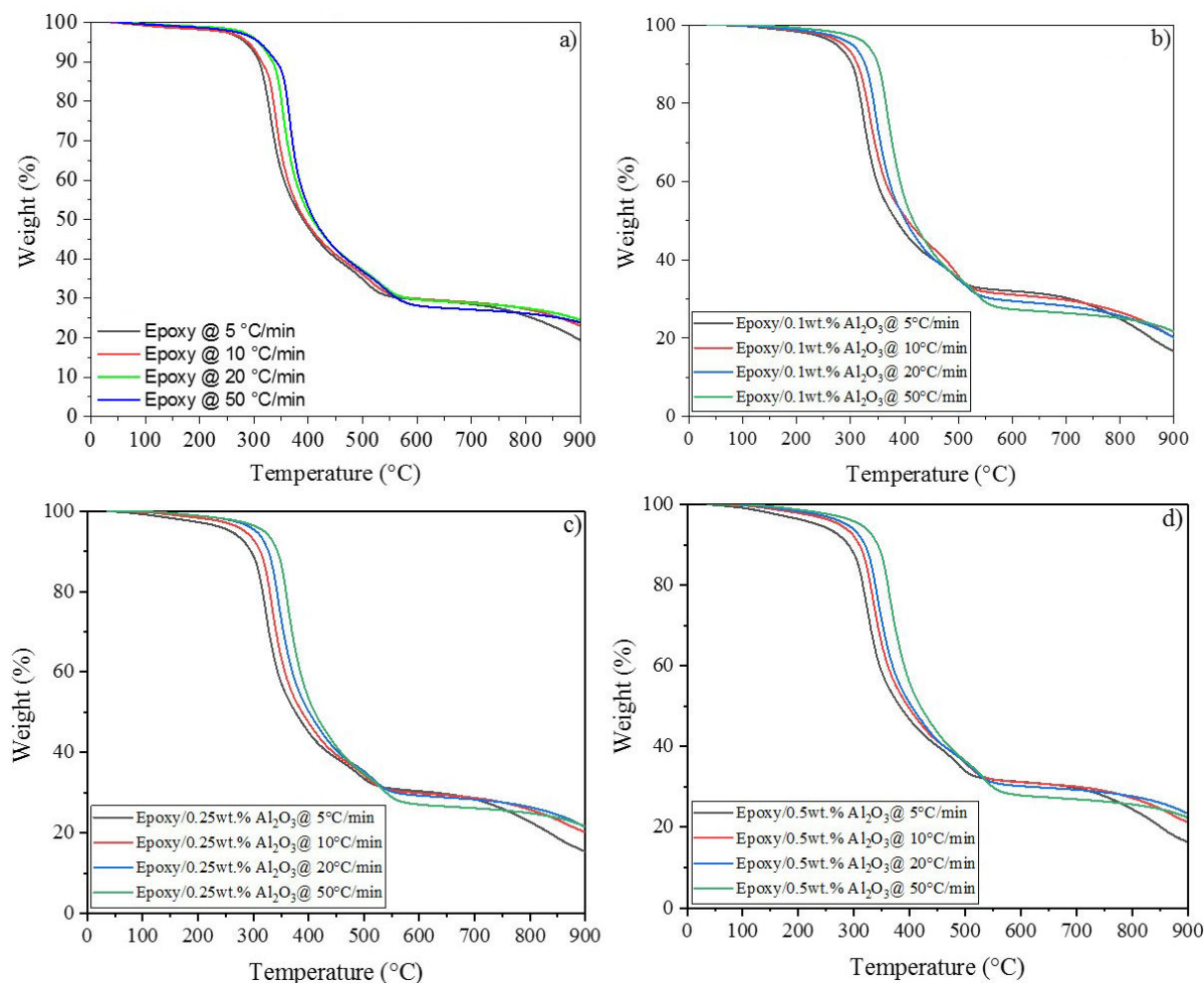
FIGURE 10. Thermograms of neat epoxy and Epoxy/Al$_2$O$_3$ at different heating ramps used to determine the kinetic degradation of the MRL method. a) Neat epoxy, b) 0.1 wt. %, c) 0.25 wt. %, and d) 0.5 wt. %.

of nano Al$_2$O$_3$ [21]. Fan-Long Jin and Soo-Jin Park [41] studied the same epoxy resin system (DGEBA) with Al$_2$O$_3$ loadings ranging from 5 up to 15 wt. %; their results show a two-stage degradation process with char increasing as the concentration of Al$_2$O$_3$ was increased [41]. However, in our case, the char yield decreased for lower concentrations of alumina by 2.88 wt. % of the total mass used in the study compared to neat epoxy. The $T_{d5}$ values remain the same until the alumina concentration reached 0.5 wt. %, at this point, the $T_{d5}$ value decreased by 15°C.

Kinetic analysis of thermal degradation was carried out with Multilinear Regression (MLR) method to fit four data curves obtained at a constant heating rate by TGA in an inert atmosphere to the Arrhenius relationship, $k(t) = A \cdot \exp(E_a/RT)$, determining the pre-exponential factor (A) (min$^{-1}$), Ea is the apparent activation energy (kJ·mol$^{-1}$), $R$ is the universal gas constant, and T is the temperature (K). For the iso-conversion method, the expression for the rate of conversion $d\alpha/dT = k(T) \cdot [1 - \alpha]^n$ can be used, where $\alpha$ is the degree of chemical conversion, $n$ is the order of reac-

tion, and $k$ is the reaction rate. The three kinetic parameters have been obtained using various iso-conversion model-free as well as MRL methods from materials data as a function of temperature and conversion. Non-isothermal TGA is one of the best methods to understand the kinetics degradation process of polymers, therefore adequate to find solutions for the estimation of the kinetic parameters [42]. The degradation kinetics analysis at different heating ramps (5, 10, 20 and 50°C/min) showed a slight displacement towards higher temperatures with higher heating ramps for the neat epoxy resin and both composites (Fig. 10 and 11). This behavior is markedly observed at temperatures below 550°C for neat epoxy, 425°C for epoxy/γ-Al$_2$O$_3$ and 475°C for epoxy/ZnO.

Figure 12 presents the activation energy ($E_a$) for all the composites and neat epoxy. Activation energy values were obtained with a determination coefficient ($R^2$) at 95 % and taken conversions of ($\alpha$) of 5, 10, 15, 20, 25, and 30 %. Ea of neat epoxy (121.53 ± 9.15 kJ/mol) and epoxy/γ-Al$_2$O$_3$ @ 0.10 % and @ 0.25 % (118.11 ± 6.47 and 104.63 ± 7.34 kJ/mol, respectively) display similar values (Zone I). How-
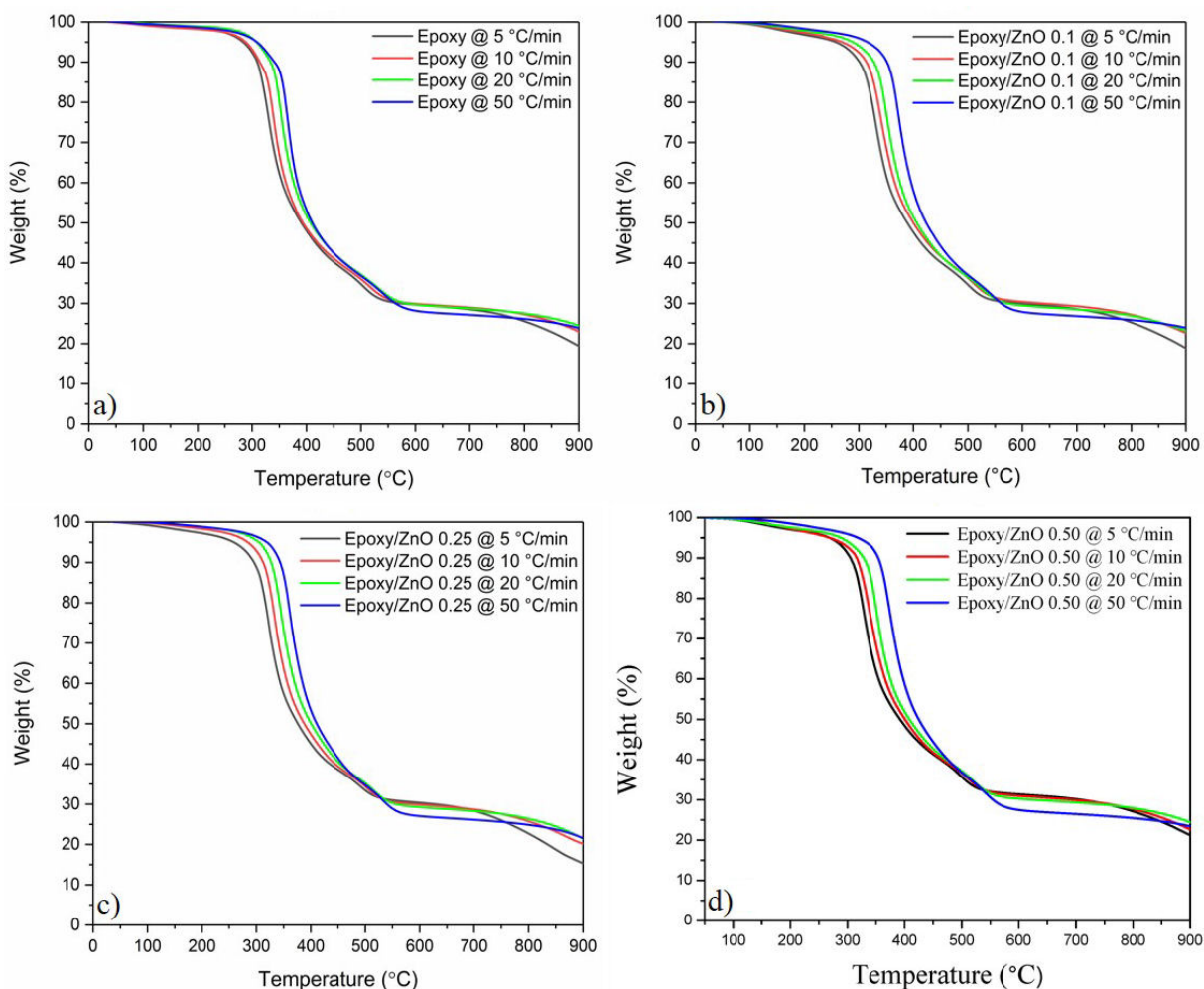
FIGURE 11. Thermograms of neat epoxy and Epoxy/ZnO at different heating ramps used to determinate kinetic degradation of MRL method. a) Neat epoxy, b) 0.1 wt. %, c) 0.25 wt. %, and d) 0.5 wt. %.
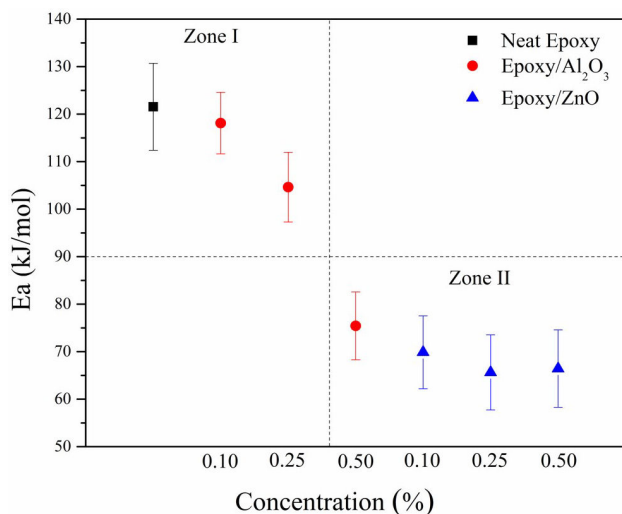


FIGURE 12. Activation energy vs. nanoparticle concentration in wt. %.

ever, a significant decrease in Ea is observed for the $\gamma$-Al$_2$O$_3$ content of 0.50 wt. % ($75.42 \pm 7.13$ kJ/mol) (Zone II). These results are in agreement with the activation energy observed by Omrani and Rostami at a similar concentration of alumina (0.5 phr) [43]. Epoxy/ZnO composites, regardless of the concentration of the filler, show similar behavior to epoxy/$\gamma$-Al$_2$O$_3$ @ 0.5 %. These results suggest that loadings $\leq 0.5$ wt. % of ZnO and only the loading of 0.5 wt. % of $\gamma$-Al$_2$O$_3$ decreased the thermal stability of neat epoxy resin. Other authors have reported decreasing activation energy values with the addition of oxide particles, mainly attributed to a catalytic effect of these particles [44,45,46]. This effect has been observed for copolymer/TiO$_2$ [44] at a concentration of 0.2 wt. % and polyacrylate/ZnO [45] composites. Therefore, the incorporation of ZnO (for all cases) and Al$_2$O$_3$ at 0.5 wt. % had a significant impact on Ea values of neat epoxy.

## 4. Conclusions

The present study analyzes the effect of the incorporation of low contents (0.1, 0.25, and 0.5 wt. %) of citrate route $\gamma$-Al$_2$O$_3$ and sol-gel synthesized ZnO nanoparticles on the thermal properties and degradation kinetics of Epolam 2500

epoxy resin. Concentrations under 1 wt. % of ceramic particles were introduced in the polymeric matrix to improve thermal behavior while maintaining the specific mechanical properties and low weight of the material.

The inclusion of $\gamma$-Al$_2$O$_3$ particles at loadings under 1 wt. % produces an evident competition between ballistic and diffusive heat transfer mechanisms, enhancing monotonically the thermal conductivity and volume-specific heat capacity of the composite as the nanoparticle content is increased at room temperature. For epoxy/ZnO, the dependence of the effective thermal conductivity on the concentration of zinc oxide particles is not monotonous. Similar behavior is obtained when calculating $C_{\text{eff}}$ of the epoxy/ZnO. The experimental results suggest that in the samples with ZnO particle additions, the ballistic mechanism also dominates over the diffusive mechanism. However, when the ZnO content reaches 0.25 wt. %, agglomeration of the particles decreases the ballistic transport, altering the monotonous behavior for that concentration.

The incorporation of $\gamma$-Al$_2$O$_3$ and ZnO particles increased the thermal stability of the polymer up to 250°C, inhibiting the first stage of thermal decomposition of the epoxy. Above 250°C, the thermal decomposition of the epoxy was accelerated by the incorporation of $\gamma$-Al$_2$O$_3$, decreasing the temperature at which the maximum rate of thermal decomposition takes place by 6°C with particle loadings of 0.5 wt. %. The addition of ZnO particles decreases the initial decomposition temperature by 19°C in the second stage of the thermal degradation of epoxy, and the Ea value decreased by 45 %.

The results suggest that the incorporation of low loadings of alumina or oxide zinc nanoparticles increases the thermal properties and thermal stability of epoxy. These results also showed a feasible manufacturing method for lightweight epoxy-based composite materials that might be used for space applications (*i.e.* nanosatellites).

## Acknowledgments

1. E. Escobar, M. Diaz and J. C. Zagal, *Appl. Therm. Eng.*, **105** (2016), 490. https://doi.org/10.1016/j.applthermaleng.2016.03.024

2. C. E. Nomme, *Mechanical Design of CubeSat Structures Using Composites and Polymers*. Master Thesis, Institutt for produktutvikling og materialer. NTNU, (2013).

3. M. A. Silva, D. C. Guerreri, A. Cervone and E. Gill, *Acta Astronaut.*, **143** (2018), 234. https://doi.org/10.1016/j.actaastro.2017.11.049

4. S. Corpino, M. Caldera, F. Nichele, N. Masoero and N. Viola, *Acta Astronaut.*, **115** (2015), 247. https://doi.org/10.1016/j.actaastro.2015.05.012

5. D. Arce, B. Jutzeler and G. Röthlisberger, Swiss Cube: Phase A Structure and Configuration (S3-A-STRU-1-4-Structure and Configuration), *Haute École Specialisée de Suisse Occidental*, LMAF (Lausanne, Switzerland, 2006).

6. A. Ampatzoglou, A. Baltopoulos, A. Kotzakolios and V. Kostopoulos, *IJASAR*, **1** (2014), 1. dx.doi.org/10.19070/2470-4415-140001

7. École Polytechnique de Laussane, *EPLF Space Center: Swiss-Cube*, (2011). [Online]. Available: http://swisscube.epfl.ch/

8. M. A. Viscio *et al., Acta Astronaut.*, **104** (2014), 516. https://doi.org/10.1016/j.actaastro.2014.06.005

9. A. Poghosyan and A. Golkar, *Prog. Aerosp. Sci.*, **88** (2017), 59. https://doi.org/10.1016/j.paerosci.2016.11.002

10. N. Saba, P. Tahir and M. Jawaid, *Polymers (Basel)*, **6** (2014), 2247. https://doi.org/10.3390/polym6082247

11. S. Fakirov, *Compos. Sci. Technol.*, **89** (2013), 211. https://doi.org/10.1016/j.compscitech.2013.10.007

12. M. Baibarac and P. Gómez-Romero, *J. Nanosci.Nano. Technol.*, **6** (2006), 289. https://doi.org/10.1166/jnn.2006.903

13. X. Zhang, H. Hao, Y. Shi, J. Cui and X. Zhang, *Constr. Build. Mater.*, **114** (2016), 638. https://doi.org/10.1016/j.conbuildmat.2015.04.057

14. Y. Li, H. Zhang, H. Porwal, Z. Huang, E. Bilotti and T. Peijs, *Compos. Part-A-Appl. S.*, **95** (2017), 229. https://doi.org/10.1016/j.compositesa.2017.01.007

15. P. Katti, K. Kundan, S. Kumar and S. Bose, *Polymer*, **122** (2017),184. https://doi.org/10.1016/j.polymer.2017.06.059

16. J. Kim, D. Seong, T. Kang and J. Youn, *Carbon*, **44** (2006), 1898. https://doi.org/10.1016/j.carbon.2006.02.026

17. H.P. Chang, H. Liu, and C. Tan, *Polymer*, **75** (2015), 125. https://doi.org/10.1016/j.polymer.2015.08.023

18. Wu, M., X. Yuan, H. Luo, C. Chen, K. Zhou and D. Zhang, *Phys. Lett. A*, **381** (19) (2017), 1641. https://doi.org/10.1016/j.physleta.2017.02.025

19. Y. Hu, G. Du and N. Chen, *Compos. Sci. Technol.*, **124** (2016), 36. https://doi.org/10.1016/j.compscitech.2016.01.010

20. L. McGrath, R. Parnas, S. King, J. Schroeder, D. Fischer and J. Lehart, *Polymer*, 49 (2008), 999. https://doi.org/10.1016/j.polymer.2007.12.014

21. W. Jiang, F.-L. Jin and S.-J. Park, *J. Ind. Eng.Chem.*, **18** (2012), 594. https://doi.org/10.1016/j.jiec.2011.11.140

22. A. Omrani, L. Simon and A. Rostami, *Mater. Chem. Phys.*, **114** (2009), 145. https://doi.org/10.1016/j.matchemphys.2008.08.090

23. M. Zakaria, H. Akil, M. Kudus and M. Othman, *Compos. Part B-Eng.*, **91** (2016), 235. https://doi.org/10.1016/j.compositesb.2016.01.013

24. S. Mallakpour and V. Behranvand, *Eur. Polym. J.*, **84** (2016), 377. https://doi.org/10.1016/j.eurpolymj.2016.09.028

25. Y. Feng, C. He, Y. Wen, X. Zhou, X. Xie, Y. Ye and W.-W. Mai, *Compos. Sci. Technol*, **160** (2018), 42.

26. M. W. Akhtar, Y. S. Lee, D. J. Yoo and J. S. Kim, *Compos. Part-B Eng.*, **131** (2017), 184. https://doi.org/10.1016/j.compositesb.2017.07.067

27. S. Gustafsson, M. Chohan and A. Magsood, *J. Appl. Phys.*, **55** (1984), 3348. https://doi.org/10.1063/1.333373

28. A. Magsood and M. Anis-ur-Rehman, 2013IOP Conference Series: *Materials Science and Engineering*, Indus University, (Pakistan, 2013).

29. S. E. Gustafsson, *Rev. Sci. Instrum.*, **62** (1991), 797. https://doi.org/10.1063/1.1142087

30. G. Paglia, Faculty of Science, *Department of Applied Physics and Department of Applied Chemistry*, Curtin University, Perth, Australia, 2004.

31. J. Chiguma, E. Johnson, P. Shah, N. Gornopolskaya and W. Jones Jr., *Open J. Compos. Mater.,* **3** (2013), 51. https://doi.org/10.4236/ojcm.2013.33007

32. Y.-X. Fu, Z.-X. He, D.-C. Mo and S.-S. Lu, *Appl. Therm. Eng.*, **66** (2014), 493. https://doi.org/10.1016/j.applthermaleng.2014.02.044

33. W. Yuan, Q. Xiao, L. Li and T. Xu, *Appl. Therm. Eng.*, **106** (2016), 1067. https://doi.org/10.1016/j.applthermaleng.2016.06.089

34. A. Mendioroz, R. Fuente-Dacal, E. Apiñaniz and A. Salazar, *Rev. Sci. Instrum.*, **80** (2009), 074904. https://doi.org/10.1063/1.3176467

35. A. Salazar, A. Mendioroz and R. Fuente, *Appl. Phys. Lett.*, **95** (2009), 121905. https://doi.org/10.1063/1.3236782

36. K. Martínez *et al.*, *Int. J. Therm. Sci.*, **98** (2015), 202. https://doi.org/10.1016/j.ijthermalsci.2015.07.019

37. J. Gu, X. Yang, Z. Lv, N. Li, C. Liang and Q. Zhang, *Int. J. Heat Mass Tran.*, **92** (2016), 15. https://doi.org/10.1016/j.ijheatmasstransfer.2015.08.081

38. A. A. Moosa, F. Kubba, M. Raad and A. Ramazani, *Am. J. Mater. Sci.*, **6** (2016), 125. https://doi.org/10.5923/j.materials.20160605.02

39. D. Gúzman, X. Ramis, X. Fernández-Franco and A. Serra, *Polymers*, **7** (2015), 680. https://doi.org/10.3390/polym7040680

40. K. Curran and M. Strlič, *Stud. Conserv.*, **60** (1) (2015), 1. https://doi.org/10.1179/2047058413Y.0000000125

41. F.-L. Jin and S.-J. Park, *Polym. Degrad. Stabil.*, **97** (2012), 2148. https://doi.org/10.1016/j.jiec.2015.03.026

42. M. Kumar, S. Sabbarwal, P. Mishra and S. Upadhyay, *Bioresource Technol.*, **279** (2019), 262. https://doi.org/10.1016/j.biortech.2019.01.137

43. A. Omrani and A. A. Rostami, *Mat. Sci. Eng. A-Struct.*, **517** (2009), 185. https://doi.org/10.1016/j.msea.2009.03.076

44. T.-K. Yang, S. S.-Y. Lin and T.-H. Chuang, *Polym. Degrad. Stabil.*, **78** (2002), 525.

45. S.-C. Liufu, H.-N. Xiao and Y.-P. Li, *Polym. Degrad. Stabil.*, **87** (2005), 103. https://doi.org/10.1016/j.polymdegradstab.2004.07.011

46. M. Ghaffari, M. Ehsani, M. Vandalvand, E. Avazverdi, A. Askari and A. Goudarzi, *Prog. Org. Coat.*, **89** (2015) 277. https://doi.org/10.1016/j.porgcoat.2015.08.016